Speckle-noise filtering based on non-local mean sparse principal component analysis method

Tounsi, Yassine ; Kumar, Manoj ; Kaur, Karmjit ; Santoyo, Fernando-Mendoza ; Matoba, Osamu ; Nassim, Abdelkrim

(Citation)
Optics and Lasers in Engineering,164:107507

(Issue Date)
2023-02-17

(Resource Type)
journal article

(Version)
Accepted Manuscript

Highlights:

1. The objective of this work is to exploit the performance of the non-local sparse principal component analysis (NLS-PCA) method for speckle noise filtering in coherent optical techniques.
2. The study shows that the proposed NLS-PCA method performs very well for speckle noise filtering and edge preservation at low computational complexity.
3. It is concluded that the method for speckle noise filtering is effective and could be established as a powerful speckle-noise filtering tool for optical imaging techniques.

Speckle-noise Filtering based on Non-local Mean Sparse Principal Component Analysis Method

Yassine Tounsi[1,†,*], Manoj Kumar[2,3,†,**], Karmjit Kaur[4], Fernando-Mendoza Santoyo[5], Osamu Matoba[2,3] and Abdelkrim Nassim[1]

[1]*ChouaibDoukkali University, Sciences Faculty, Department of Physics, Benmaachou street, El Jadida, Morocco,24000.*
[2]*Kobe University, Graduate School of System Informatics, Department of Systems Science, Rokkodai 1-1, Nada, Kobe 657-8501, Japan*
[3]*Center of Optical Scattering Image Science, Kobe University, Rokkodai 1-1, Nada, Kobe 657-8501, Japan*
[4]*Govt. P.G. College, Ambala Cantt. Haryana 133001, India*
[5]*Centro de Investigaciones en Optica, A.C., Leon, Guanajuato, Mexico 37160*

† The authors contributed equally to the work.

* yassinetounsi132@gmail.com

** manojklakra@gmail.com

Abstract

Speckle-noise filtering is an extensive and key process in coherent interferometric techniques to obtain important and accurate information from the recorded interferogram or fringe pattern. The speckle-noise inherent to these interferograms, recorded by digital image sensors in these optical techniques, is eliminated by an appropriate image processing method. Since the beginning and further development of these techniques, a wide variety of speckle noise filtering methods and techniques have been proposed. The present research work aims to exploit the performance of the non-local sparse principal component analysis (NLS-PCA) method for speckle noise reduction as applied to the interferometric fringe patterns obtained from digital holographic and digital speckle pattern interferometric techniques. The performance of the NLS-PCA is evaluated on numerical simulations using different types of speckle fringe patterns resulting in the method being highly effective in filtering the speckle noise and providing superior results evaluated in terms of peak signal-to-noise ratio (PSNR), structural similarity index (SSIM), Edge preservation Index (EPI), and Equivalent Number of look (ENL), in comparison to widely known methods such as windowed Fourier transform method, Lee filter, Weiner filter. Furthermore, the proposed method maintains the finer details and preserves the fringe edges effectively. The performance of the NLS-PCA method is also demonstrated on experimental speckle fringe patterns and digital holograms.

Keywords: Speckle noise; Digital speckle pattern interferometry; Digital holography; Principal component analysis.

1. Introduction

Laser-based optical imaging including microscopy [1-13] and measurement techniques [14-22] are the incontestable vital tools that have become increasingly important for various scientific, engineering, and industrial applications. Interferometric techniques including digital holography (DH) [23], digital speckle pattern interferometry (DSPI) [24], and shearography [25] are widely used optical measurement techniques based on coherent imaging systems. Unfortunately, the resultant fringe patterns carry high-frequency speckle noise due to the

coherence nature of the light source (i.e. a laser) used in these techniques. The presence of speckle noise affects fine details and edges which limits the contrast resolution and adds ambiguity to the measurements. In short, speckle noise degrades the visual evaluation and makes diagnosis inaccurate and more difficult. The analysis of these recorded fringe patterns for the determination of physical measurands requires a speckle noise filtering step in order to obtain a high-quality phase map, consequently, for the efficient physical measurand precision. Therefore, in these techniques, the speckle noise filtering step is always needed before data processing. The main challenge in speckle filtering is to preserve all the fine details and the edges of the processed images/fringe patterns.

A variety of speckle noise filtering techniques have been proposed in diverse research fields such as speckle metrology [26], medical imaging [27], and synthetic aperture radar (SAR) imaging [28]. Generally, speckle noise filtering techniques are categorized as hardware-based and software-based approaches [26]. However, a software-based approach (i.e. based on image processing) is considered to be an efficient and economical way of speckle noise reduction in optical techniques. The speckle noise filtering methods, based on the image processing approach, can further be classified mainly into spatial-domain, transform-domain, and hybrid methods. Each method has advantages and limitations, as we have discussed in detail in our previous paper [26]. The field of fringe pattern filtering by image processing is always an active research area aiming to propose and improve the existing methods to provide superior results with high quality and information preservation at the edges.

Over the years, a large variety of methods and approaches has been published on speckle filtering is introduced. Boumbach et al. [29] Introduced an approach based on the use of several recorded holograms of the same specimen for the reconstructed phase map quality improvement. Whereas, Rong et al. [30] proposed another approach where multiple off-axis

holograms are recorded using a circularly polarized illumination beam and a rotating linearly polarized reference beam, and the speckle noise is removed in the reconstructed images by averaging these fields. Zhou and Li exploited the bidimensional empirical mode decomposition for DSPI fringe denoising [31]. Xiao et al. [32] introduced an improved variational mode decomposition for DSPI phase map denoising, in this work, the authors proposed an adaptive mode threshold method to process the obtained optimal mode components given after the variational mode decomposition of the input DSPI phase map. Kemao [33] introduced a frequency-based method package called windowed Fourier transform for DSPI fringe despeckling and analysis. Other researchers as Yassine et al. [34], Ning et al. [35] introduced a wavelet transforms-based approach, this approach gives accurate results according to the mother wavelet and the scale of decomposition. In the same context, Zada et al. [36] proposed an approach that combines wavelets transform and monogenic signal called monogenic wavelets transform. Another efficient method called Block Matching 3D introduced by Dabov et al. [37] in 2006 is recognized as the state of the art in image processing, this method combines efficient denoising techniques and synthesizes the most major advances that occurred in recent years. Tounsi et al. [38,39] exploited in detail the power of nonlocal mean and its adaptive related kernels for denoising speckle fringes.

The purpose of this work is to adopt the non-local sparse principal component analysis (NLS-PCA) method with some significant modifications and use it for the filtering of speckle noise in DSPI and DH. The method was introduced by Salmon et al. [40] for Poisson noise removal in 2014. The principal component analysis (PCA) method gained a great interest in image processing, specifically in image filtering. The general idea of the PCA denoising-based method is to transform the original dataset into a PCA domain preserving only the most important principal components, i.e., this time the noise and any trivial information can be removed. The first exploitation of the PCA for image filtering was realized by Muresan and Parks [41], in

which the authors proposed a spatially adaptive PCA-based speckle noise filtering procedure. The schema used by Muresan and Parks is realized on noise filtering by using a moving window to compute the local statistics from which the PCA matrix is estimated. However, the filtering procedure is applied directly to the PCA transformation to the noisy image without any data selection, and this makes some residual noise and visual artifacts appear in the filtered image. Lv et al. [42] introduced a novel approach called multilinear PCA (MPCA) to denoise multi-frame optical coherence tomography (OCT) data. In this method, the nonlocal similar 3D blocks extracted from the data are first grouped using the k-means clustering method in order to well preserve local image features. After that, the MPCA transform is performed on each group and the transform coefficients are shrunk to remove speckle noise. Finally, the filtered OCT volume is obtained by inverse MPCA transform and aggregation. A new hybrid speckle noise filtering method, based on Undecimated Dual-Tree Complex Wavelet Transform (UDT-CWT) and non-local Principal Component Analysis (PCA) with local pixel grouping (LPG-PCA) on SAR images, is proposed by Ramin Farhadiani et al. [43]. Furthermore, different variants of PCA methods have become widespread in image filtering techniques including patch-based PCA [44], patch-based global PCA (PGPCA) [45], and patch-based hierarchical PCA [46] , to name a few.

The above gives an updated account of the NLS-PCA method for speckle noise filtering in DSPI and DH. The second and third sections present a detailed explanation of the filtering concept of NLS-PCA, and the fourth section will focus on the principal findings and results obtained from filtering using numerical simulation and experimentally obtained speckle fringe patterns and a digital hologram of a dice.

2. Principal component analysis (PCA)

Consider an image patch e^1 in the image and $n-1$ most similar nonlocal image patches e^j, with $j = 2, 3,\ldots,n$, can be found in the entire image (called a search window). Then, group these vectors into a matrix E which is expressed as:

$$E = \begin{bmatrix} e_1^1 & e_1^2 & . & . & . & e_1^n \\ e_2^1 & e_2^2 & . & . & . & e_2^n \\ . & . & . & . & . & . \\ . & . & . & . & . & . \\ . & . & . & . & . & . \\ e_m^1 & e_m^2 & . & . & . & e_m^n \end{bmatrix} \tag{1}$$

where e_i^j is the j^{th} entry of vectorized image patch i. The j^{th} row of the sample matrix E is denoted by

$$E_i = \begin{bmatrix} e_i^1 & e_i^2 & \ldots & e_i^n \end{bmatrix} \tag{2}$$

which is called the sample vector of e_i.

The mean value of E_i is computed as:

$$\mu_i = \frac{1}{n}\sum_{j=1}^{n} E_i(j) \tag{3}$$

The sample vector is centralized as

$$\overline{E_i} = E_i - \mu_i = \begin{bmatrix} \overline{e_i^1} & \overline{e_i^2} & \ldots & \overline{e_i^n} \end{bmatrix} \tag{4}$$

where $\overline{e_i^j} = e_i^j - \mu_i$.

Accordingly, the centralized matrix of E is

$$\overline{E} = \begin{bmatrix} \overline{E_1}^T & \overline{E_2}^T & \ldots & \overline{E_m}^T \end{bmatrix}^T \tag{5}$$

where T is the transpose operator. Finally, the co-variance matrix of the centralized dataset is calculated as

$$\Omega = \frac{1}{n}\overline{E}\,\overline{E}^T \tag{6}$$

The goal of PCA is to find the orthonormal transformation matrix P to de-correlate $\overline{E}$, i.e., $\overline{F} = P\overline{E}$, so that the co-variance matrix of $\overline{F}$ is diagonal. Since the co-variance matrix Ω is symmetrical, it can be written as:

$$\Omega = \Phi \Lambda \Phi^T \tag{7}$$

where $\Phi = [\emptyset_1\ \emptyset_2\ \emptyset_3 \ldots \emptyset_m]$ is the $m \times m$ orthonormal eigenvector matrix and $\Lambda = diag\{\lambda_1, \lambda_2, ..., \lambda_m\}$ is the diagonal eigenvalue matrix with $\lambda_1 \geq \lambda_2 \geq ... \geq \lambda_m$. The terms $\emptyset_1\ \emptyset_2\ \emptyset_3 \ldots \emptyset_m$ and $\lambda_1, \lambda_2, ..., \lambda_m$ are the eigenvectors and eigenvalues of Ω. By setting $P = \Phi^T$, $\overline{E}$ can be de-correlated. An important property of the PCA is that it fully de-correlates the original dataset $\overline{E}$. Generally speaking, the energy of a signal will concentrate on a small subset of the PCA-transformed dataset, while the energy of noise will evenly spread over the whole dataset. Therefore, the signal and noise can be better distinguished in the PCA domain.

3. Non-local sparse principal component analysis filtering method (NLS-PCA)

The entire procedure of the NLS-PCA filtering is summarized in Figure 1. The procedure begins with the creation of a small noisy image called a patch (of size h) according to the principle of the non-local means (NLM) algorithm [38], [39], [47]. Then, the clustering step consists of creating a number of clusters of patches. The clustering step is based on a geometrical partitioning of the image and it is a robust approach that avoids dissimilar regions in the image: for this method, the clustering step is performed in the patches domain which remains in the non-local approach. The clusters defined by $P^1, P^2, P^3, \ldots, P^N$ in the figure below are the segmented patch image intensities.

The third step deals with the filtering of clusters, the approach of filtering employs an adopted PCA for speckle noise filtering. The filtering of the clusters consists of the following steps:

- Learning an orthogonal basis from the noisy clusters by performing PCA and decomposing these noisy clusters on this basis.
- The denoised clusters are obtained by thresholding all small coefficients in the representation of the noisy clusters on a learned basis. This procedure is similar to wavelets filtering [34].

The fourth step deals with the fusion of the denoised clusters in order to obtain the denoised patches. Once the collection of patches is denoised, it will be reprojected into the pixel domain and reconstructs the final denoised fringe pattern. The reprojection creates the passage from the patches to spatial domains.

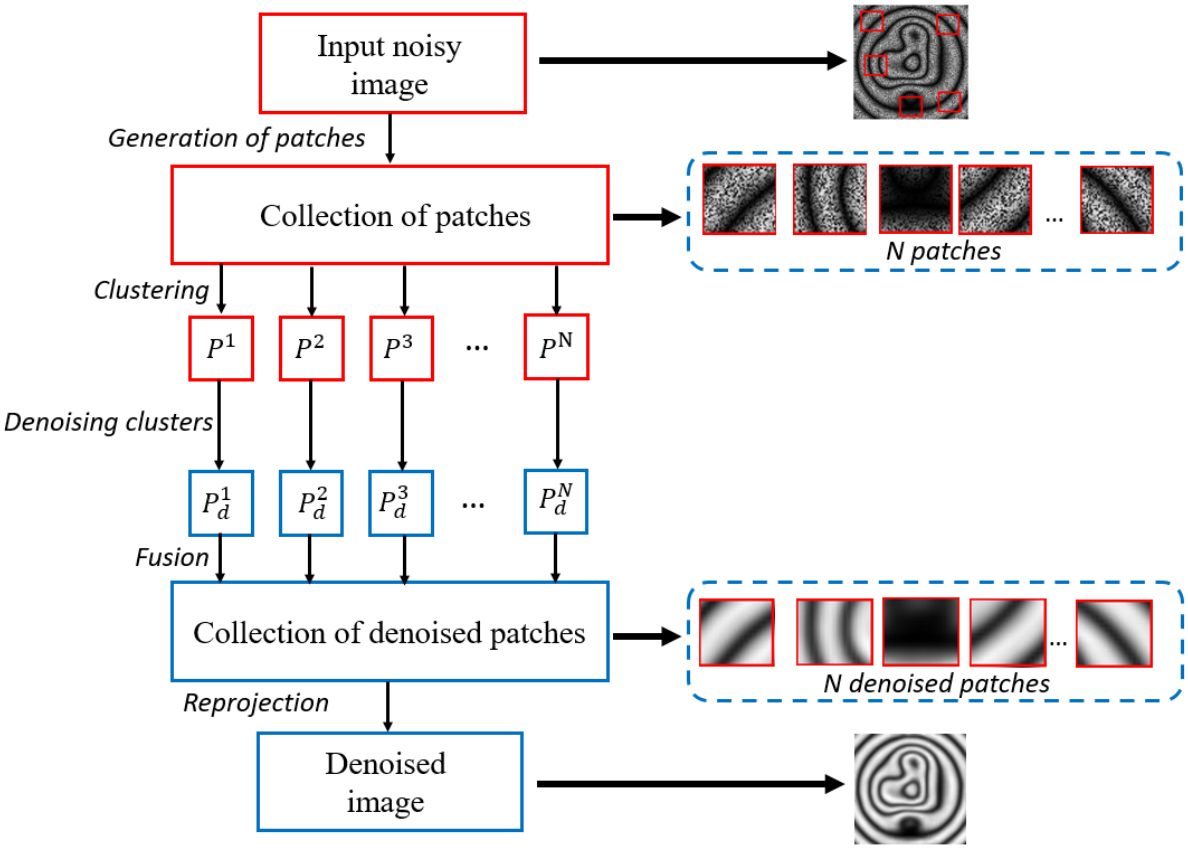

Fig. 1. Visual summary scheme of the NLS-PCA speckle noise removing method.

There are various techniques to reproject information from patches to pixels, a detailed description is provided in our previous work [39]. In this study, we use a uniform average of all the good patch candidates [39].

4. Results and Discussions

The performance of NLS-PCA method for speckle noise filtering is performed first on computer-simulated speckle fringe patterns and then on experimentally recorded data. The simulated speckle fringe patterns are generated following the method reported by Barj et al. in [48]. The simulated fringe patterns are shown in Fig. 2 which are simulated with a resolution of 256×256 on a scale of 256 gray levels, and for different fringe densities (with fringe numbers: 5, 8, 11, 16, 26). In interferometric measurements, the high density of fringes (more fringes) results from more changes occurring in the test object and it may induce high noise in the measuring signal and makes analysis more difficult. Therefore, the varying fringe densities are very important for studying the performance of a filtering method because the high fringe density affects noise reduction and as a consequence the accuracy of the fringe analysis. There may require to optimize some parameters of a filtering method for high-density and low-density fringes. So, in the proposed method, the first step is to fix the same parameters for both methods (Non-Local Sparse-PCA and Non-Local-PCA), and implement the filtering. The principal parameters are the patch width denoted by h and the number of clusters denoted by c, generated by the K-means method which is an unsupervised machine learning algorithm for clustering (the symbol 'K' defines the number of pre-defined clusters that need to be created in the process). The parameter h is related to the NLM approach and its value affect directly the quality of denoising [38]. We have taken $h=5$ and varied the number of created clusters (e.g., c=50; c=70; c=100) with 15 iterations. The 15 iterations were found to be sufficient as the decrease in the background noise value is negligible beyond 15 iterations which were checked by comparing the SNRs for different iterations. The SNR for a filtered image for 15 iterations, 20 iterations, and 25 iterations are 3.22, 3.35, and 3.46, respectively. In addition, if the iteration number increase, the computational complexity increases without any significant improvement in terms of SNR.

The obtained filtering results for each cluster number for both methods (NLS-PCA, top row, and NL-PCA, bottom row) are presented in Figure 3 (for c=50), Figure 4 (for c=70), and Figure 5 (for c=100). Also, the filtered results of different methods are quantitatively evaluated based on the local zones corresponding to the red rectangle regions in the filtered images in Figs. 3-5. For quantitative appraisal, image quality metrics must be used to show the performance of the method. Peak signal-to-noise ratio (*PSNR*), Structural SIMilarity index (*SSIM*), edge preservation index (*EPI*), and equivalent number of looks (*ENL*) [49] are four important metrics for the evaluation of fringe pattern filtering quality [26].

Fig. 2. Simulated speckle fringe patterns with different fringe densities where the fringe number increases from left to right from 5, 8, 11, 16 to 26.

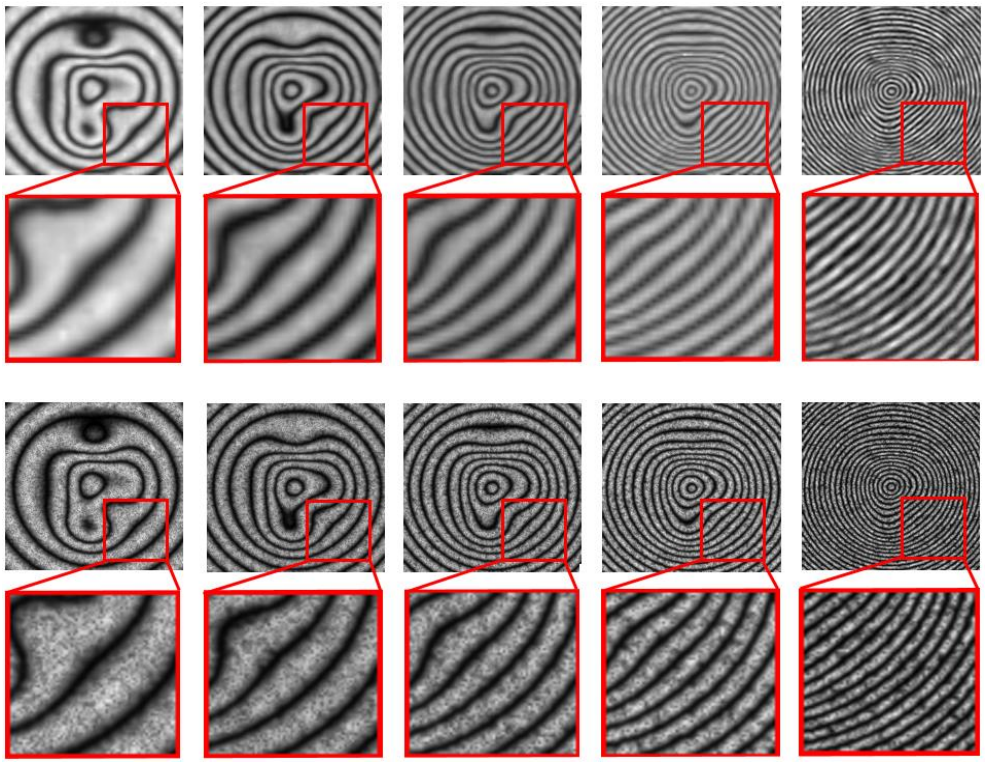

Fig. 3. Denoised speckle fringe pattern and their corresponding zooms of the red rectangle region for **c=50** using NLS-PCA (top two rows) and NL-PCA (bottom two rows).

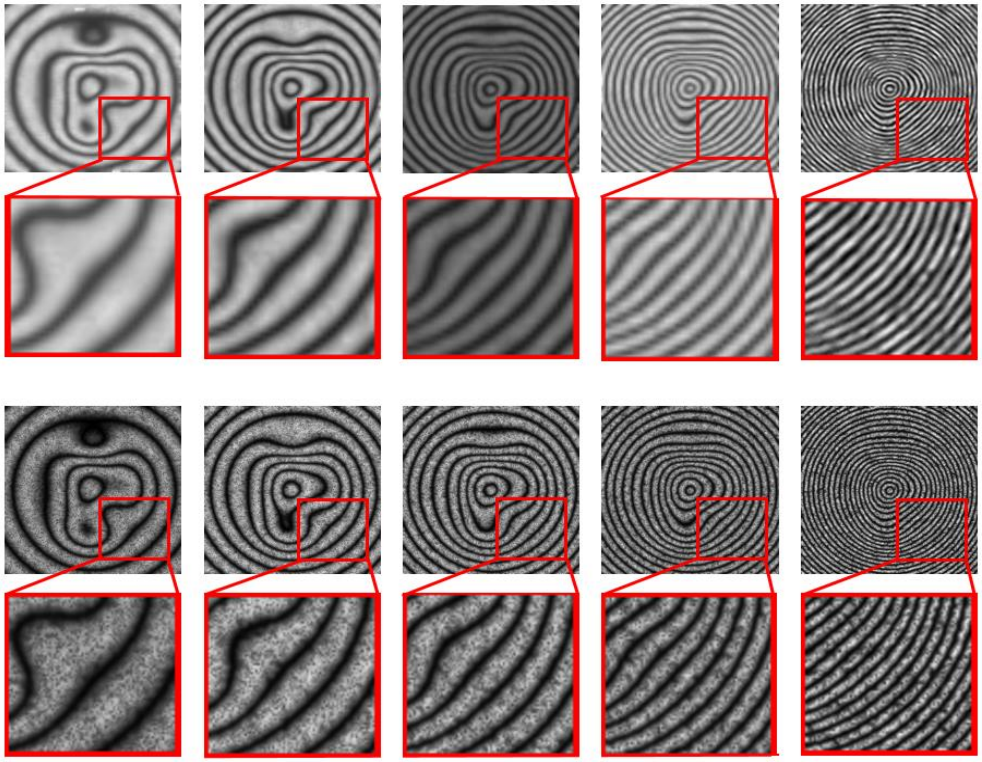

Fig. 4. Denoised speckle fringe pattern and their corresponding zooms of the red rectangle region for **c=70** using NLS-PCA (top two rows) and NL-PCA (bottom two rows).

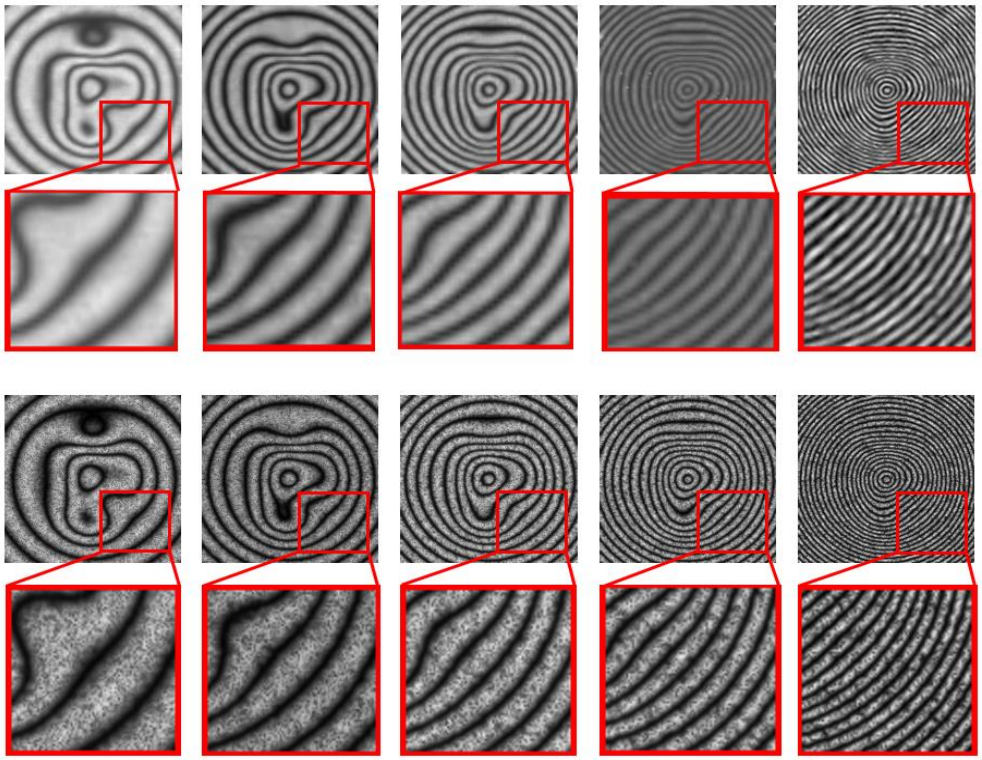

Fig. 5. Denoised speckle fringe pattern and their corresponding zooms of the red rectangle region for **c=100** using NLS-PCA (top two rows) and NL-PCA (bottom two rows).

The *PSNR* computes the peak signal-to-noise ratio between the perfect clean and the denoised fringe pattern and the higher PSNR value indicates a better quality of noise removal. is defined

as the ratio between the maximum possible power of a signal and the power of filtered noise and is given by:

$$PSNR(f_{out}, f) = 10\log_{10}\left(\frac{L^2}{MSE(f_{out}, f)}\right) \tag{8}$$

where $L=2^8-1=255$ is the maximum possible value of the image pixels when pixels are represented using 8-bits per sample; and $MSE(f_{out}, f)$ represents the mean square error between noised and denoised speckled fringe correlation defined as:

$$MSE(f_{out}, f) = \frac{1}{N.M}\sum_{i=1}^{N}\sum_{j=1}^{M}\left[f(i,j) - f_{out}(i,j)\right]^2 \tag{9}$$

where f is the original image value at pixel (i,j), f_{out} the denoised image, and M, N represents the image size.

The SSIM metric compares two input images (the perfect clean fringe pattern and the denoised fringe pattern) by extracting three features from these input images: luminance, contrast, and structure.

$$SSIM(f_{out}, f) = \frac{\left(2\mu_{f_{out}}\mu_f + C_1\right)\left(2\sigma_{f_{out}f} + C_2\right)}{\left(\mu_{f_{out}}^2 + \mu_f^2 + C_1\right)\left(\sigma_{f_{out}}^2 + \sigma_f^2 + C_2\right)} \tag{10}$$

where $\mu_{f_{out}}$ and μ_f represent the mean intensity of the denoised and noised image respectively, $\sigma_{f_{out}}$ and σ_f represent the standard deviation of denoised and noised images, respectively, $\sigma_{f_{outf}}$ is the correlation coefficient between the two input images f and f_{out}, and $C_1 = k_1L$, $C_2 = k_2L$ are two constants [where $k_1 = 0.01$ and $k_2 = 0.03$, L is the dynamic range of the pixel-values (typically this is $2^{\text{number of bits per pixel}}-1$)]. The values of SSIM are within the range [0,1] where the value of 1 indicates that the two (input and output) images are perfectly similar and the value of 0 means that the two images are very different. The third metric is *EPI*, measuring the ability of any filtering algorithm to preserve and maintain details at edges. The expression of *EPI* is:

$$EPI(f_{out}, f) = \frac{\sum_{i=1}^{m}\sum_{j=1}^{n-1}\left|f_{out}(i,j+1) - f_{out}(i,j)\right|}{\sum_{i=1}^{m}\sum_{j=1}^{n-1}\left|f(i,j+1) - f(i,j)\right|} \quad (11)$$

The values of *EPI* are in the range [0,1] where the value of 1 means that the filtering method preserves perfectly the edges.

The *ENL* of an image is defined as:

$$ENL(f) = \frac{\mu_f^2}{\sigma_f^2} \quad (12)$$

The *ENL* computes the ratio between the mean gray level of the image and the standard deviation, The larger the *ENL* value, the smoother the image.

The three presented metrics are computed for each cluster number *c*. Table 1 and Table 2 summarize the computed metrics values for NLS-PCA and NL-PCA methods, respectively, and Fig. 6 depicted these metrics values in graphical representation.

Table 1: Performance of NLS-PCA filtering method

		Fringe number	PSNR	SSIM	EPI	ENL
NLSPCA	***h*=5; *c*=50**	5	26.5	0.93	0.99	6.22
		8	16.74	0.89	0.98	5.46
		11	14.98	0.82	0.98	8.08
		16	19.03	0.85	0.97	14.62
		26	18.33	0.82	0.98	14.62
	***h*=5; *c*=70**	5	20	0.84	0.98	11.33
		8	18.89	0.89	0.98	7.26
		11	10.57	0.58	0.98	9.52
		16	19.92	0.87	0.97	15.42
		26	18.02	0.80	0.98	14.73
	***h*=5; *c*=100**	5	20.07	0.86	0.99	11.6
		8	16.15	0.86	0.99	6.35
		11	17.19	0.87	0.99	8.45
		16	12.38	0.50	0.95	18.26
		26	11.62	0.55	0.97	16.30

Table 2: Performance of NL-PCA filtering method

		Fringe number	PSNR	SSIM	EPI	ENL
NLPCA	***h*=5; *c*=50**	5	14.52	0.61	0.91	3.8
		8	13.27	0.66	0.89	3.74
		11	13.02	0.70	0.87	3.57
		16	14.02	0.76	0.84	3.35
		26	12.30	0.69	0.82	3.13
	***h*=5; *c*=70**	5	11.73	0.55	0.90	3.58
		8	13.80	0.67	0.88	3.6
		11	12.74	0.69	0.86	3.44

		16	12.63	0.72	0.83	3.42
		26	10.55	0.68	0.80	4.09
	***h*=5; *c*=100**	5	13.44	0.58	0.89	3.5
		8	12.05	0.61	0.87	3.52
		11	13.60	0.70	0.85	3.58
		16	13.36	0.73	0.82	3.37
		26	10.94	0.62	0.79	4.5

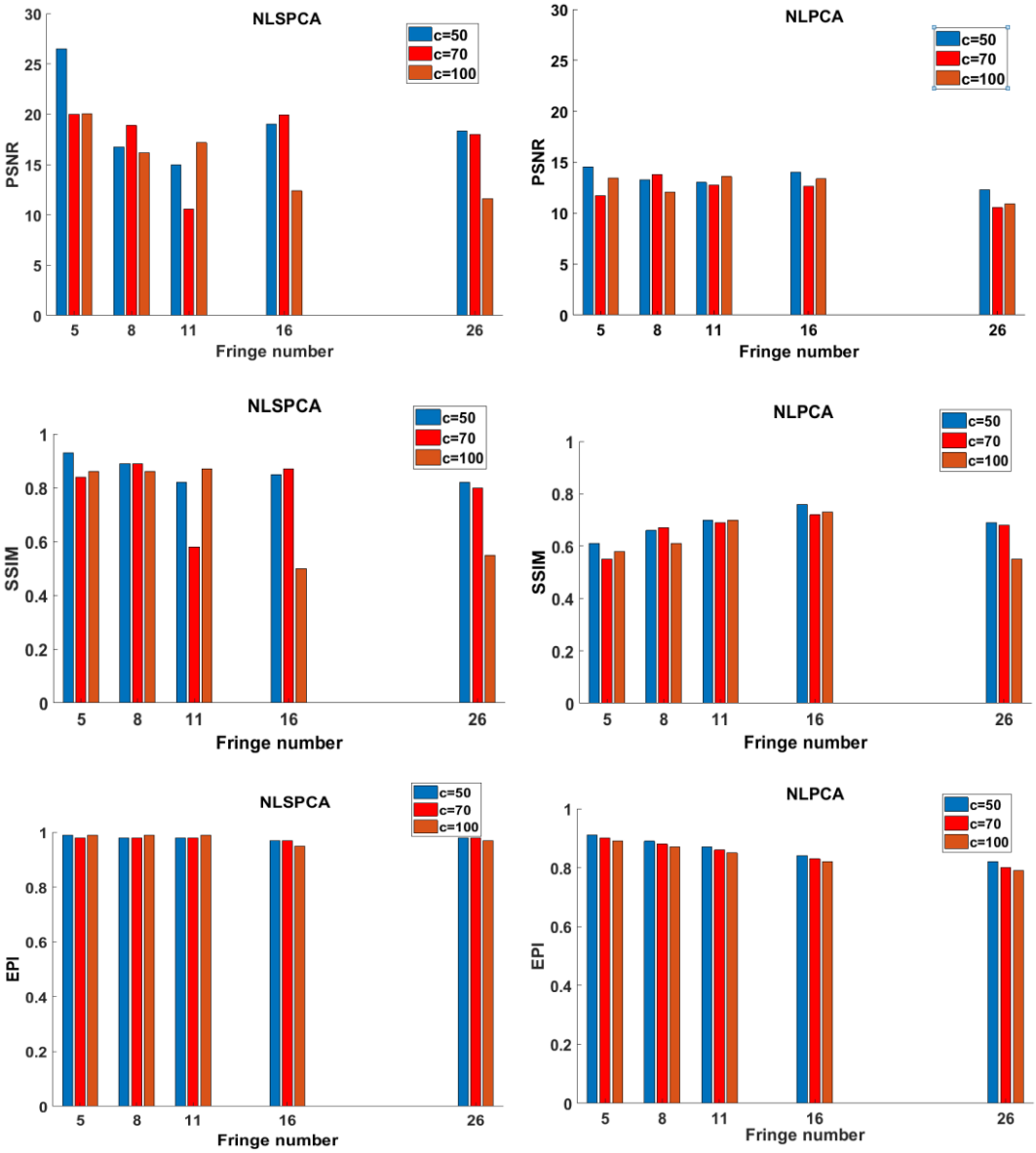

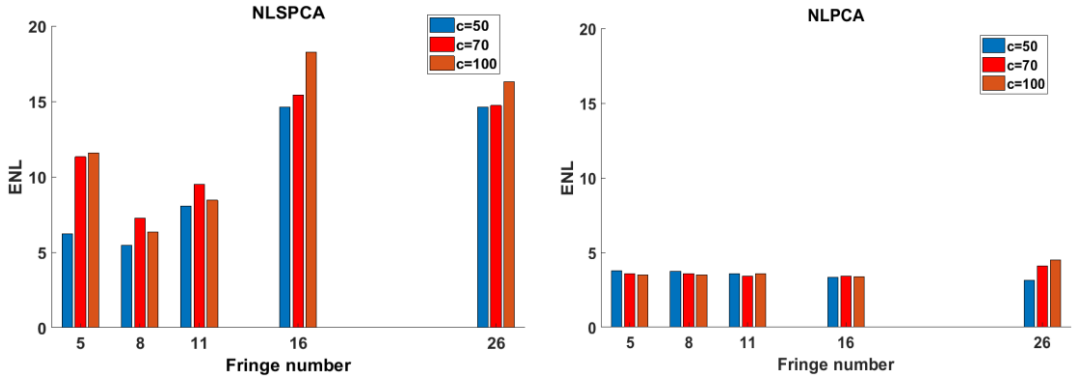

Fig. 6. Performance of NLSPCA and NLPCA in terms of PSNR (top graphs), SSIM (first middle graphs), EPI (second middle graphs), and ENL (bottom graphs) for different c values. Data were taken from tables 1 and 2.

The performance of some other speckle fringe pattern filtering methods such as the Lee filter, Windowed Fourier transform and Weiner filter is compared with the proposed method in terms of the tree metrics (PSNR, SSIM, and EPI) and presented in table 3. The parameters for these methods are: Lee filter (Window size 7*7); WFT (Default parameters in the Matlab Code written by Prof. Q. Kemao based on his work) and Weiner filter (Window size 7*7). From the obtained values of these metrics (by comparing values in Table 1 and Table 3), it can be concluded that the NLS-PCA method is more effective and feasible for speckle noise filtering.

Table 3: Performance of Lee filter, WFT and Weiner filter.

	Fringe number	PSNR	SSIM	EPI
Lee filter	5	19.22	0.85	0.98
	8	19.37	0.88	0.97
	11	16.54	0.86	0.96
	16	18.71	0.83	0.92
	26	14.26	0.62	0.88
WFT	5	16.86	0.82	0.92
	8	17.10	0.87	0.91
	11	16.94	0.89	0.91
	16	17.98	0.81	0.87
	26	17.06	0.79	0.88
Weiner filter	5	15.84	0.67	0.91
	8	16.34	0.74	0.91
	11	15.00	0.74	0.89
	16	15.94	0.59	0.80
	26	10.22	0.45	0.55

The superior performance of NLS-PCA as compared to NL-PCA is confirmed by the four computed metrics (see Table 1, Table 2, and Figure 6). This performance is due to the sparsity approach attached to the PCA technique. It is known that the classic PCA has major practical

and theoretical drawbacks when it is applied to high-dimensional data [50] (two-dimension in this case). The principal loading components are typically nonzero which makes it difficult to interpret them and identify the important variables. To overcome this drawback, the sparsity approach formulates the PCA as a regression-type optimization problem and consequently obtains sparse loading by imposing the lasso or elastic net penalty on the regression coefficients [51]. The sparsity approach reduces the time of filtering. The time taken by each method to execute the process of denoising is computed as reported in table 4. The NLS-PCA performs filtering between 3 to 5 seconds for the different input speckle fringe patterns presented in Figure 1, whereas, the NL-PCA approach performs filtering between 11 and 15 seconds.

Table 4: Computational time of different denoising methods

Denoising method	**Time of computation (s)**
NLPCA (*c*=20)	22.6
NLPCA (*c*=70)	18.2
NLPCA (*c*=100)	13.5
NLSPCA (*c*=20)	**3.75**
NLSPCA (*c*=70)	**3.3**
NLSPCA (*c*=100)	**3**
Lee filter	6.9
Weiner filter	8.4
WFT	9.3

Furthermore, the important parameters in the proposed NLSPCA method are c (number of clusters) and h (patch size). The obtained results and the quantitative appraisal are realized for different values of these parameters (c and h) for denoising implementation using the proposed NLSPCA method. We evaluated the PSNR and the SSIM of the obtained results by NLSPCA for h = {5;10;15;20} and c = {10,20,30,….,100}. The two plots shown in Figure 7 represent the effect of the two parameters on denoising performance. Therefore, to obtain the best filtering results, their parameters need to be optimized for a particular input noisy image.

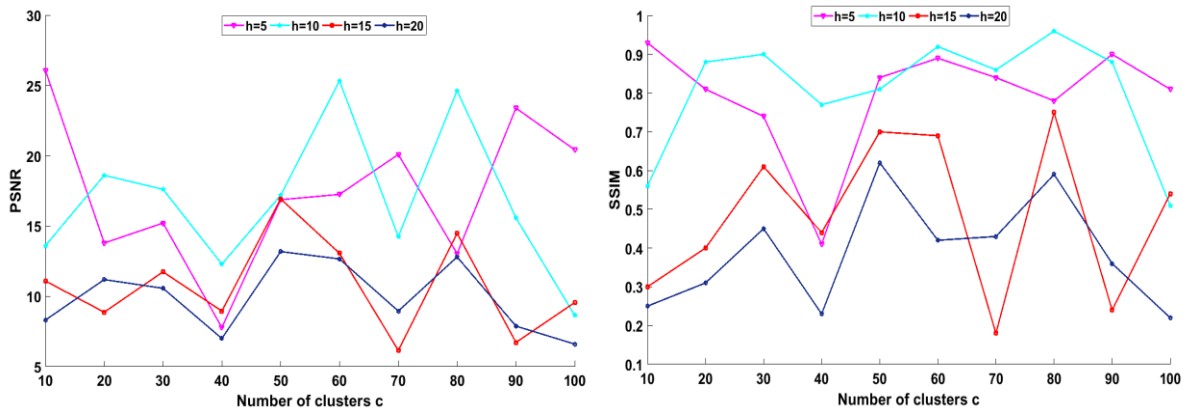

Fig 7: Performance of NLSPCA in terms of PSNR and SSIM for several patch sizes and number of clusters.

To illustrate the performance of the NLS-PCA method for speckle noise filtering when experimental data are processed, we analyzed a real recorded speckle fringe pattern and a two-dice image reconstructed from an experimentally recorded digital hologram. The performance of the NLS-PCA is evaluated on the experimentally obtained interferograms by the DSPI [24] and DH [52] setups. The experimental setups of the DSPI and DH are depicted schematically in Figs. 8 and Figs. 9, respectively. In DSPI, the He–Ne laser (power 15 mW) is split into reference and object beams by the beam splitter, BS1. The object beam is expanded by a beam expander, BE, which illuminates the surface of the object under study and produces the speckle field. The speckled image is formed on the image sensor [CCD sensor, 640 pixels×640 pixels; pixel size − 9 μm] by the imaging lens, L. The reference beam is spatially filtered by the spatial filter, SF, and collimated by the collimator, C, before interfering with the object beam at the beam combiner, BS_2. The speckle interferogram formed by the combination of object and reference beams was recorded. Two speckle interferograms corresponding to the two different states of the object are recorded in DSPI and then subtracted to obtain the DSPI fringes. Figure 10(a) shows a processed DSPI fringe pattern.

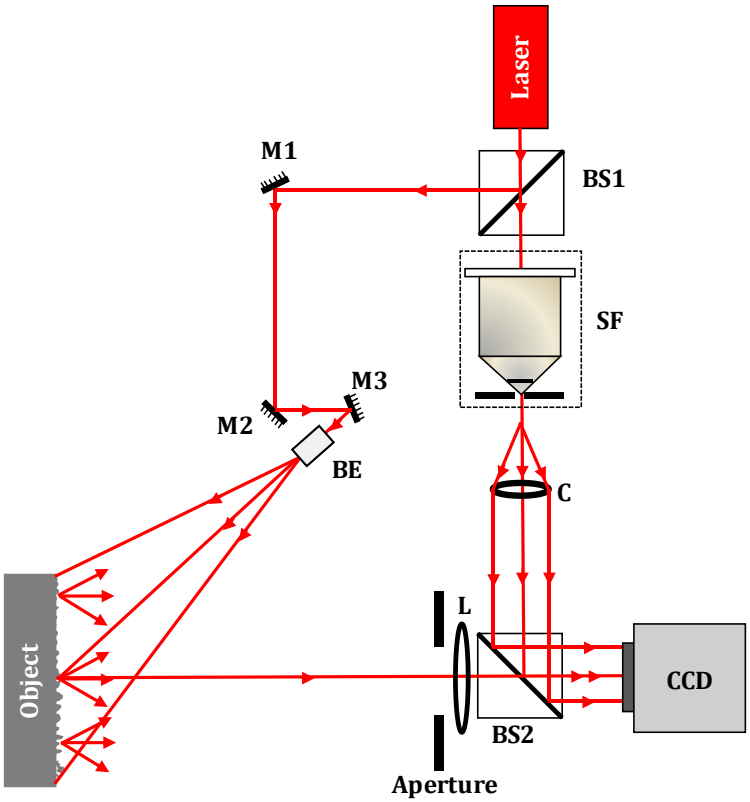

BS – Beam splitter; BE – Beam expander; C – Collimator; L – imaging lens; M – Mirror; SF – Spatial filter

Fig. 8: Schematic of the DSPI setup [24].

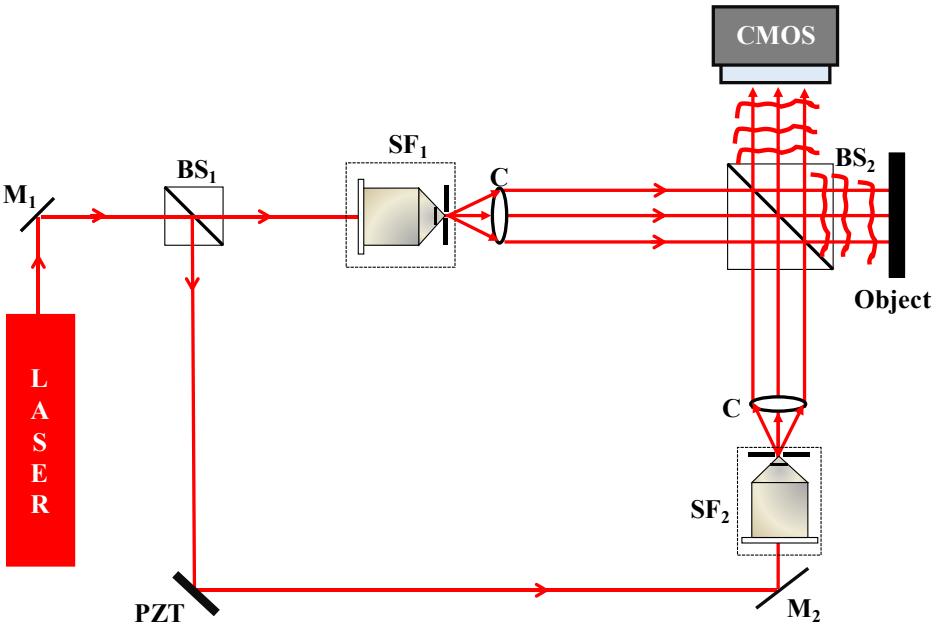

M_i – Mirrors, BS_i – Beam Splitter, SF_i – Spatial Filters, C – Collimator

Fig. 9: Schematic of the digital holography reflection setup based on the Mach–Zehnder interferometer, modified from [52].

The denoising performance of these methods is also verified on the two-dice image, numerically reconstructed from the experimentally recorded digital hologram from a phase-shifting Mach–Zehnder type digital holographic (DH) setup (as obtained from an open-access database [52]). The recording setup of DH comprises a Mach–Zehnder type interferometer working in the reflection mode. In the experimental setup, a laser beam of a wavelength of 632.8 nm and power of 5mW is used. The laser beam is divided into the object and reference beams by using a beam splitter, BS_1, and spatially filtered (by SF_1 and SF_2) and collimated by the collimators (C). The beam reflected from the object and the clean reference beam are combined by using another beam splitter, BS_2, and form a digital hologram, recorded by an image sensor. Each hologram is a combination of four phase-shifted interference patterns that are sequentially recorded, with a constant phase step of $\pi/2$, adjusted by a computer-controlled piezo-electric mirror in the reference beam. From the recorded digital holograms, the real and virtual object waves can be reconstructed if the diffraction of the reference wave is carried out by numerical methods.

Figures 10(a) and 11(a) show the experimental data from the DSPI and DH, respectively. Figures 10(b-f) and 11(b-f) present the resulting filtered images using the NLS-PCA, NLPCA, Lee filter, Weiner filter, and WFT, respectively. Since there are no reference images for these experimentally obtained images, therefore, the equivalent number of looks (ENL) is computed for all the images [Fig. 10(a-f) and Fig. 11(a-f)].

(a) (b) (c)

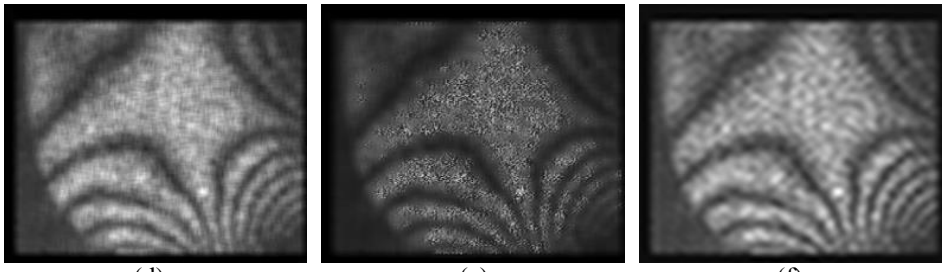

(d) (e) (f)

Fig. 10. Results of filtering for real DSPI fringes. (a) Original image, (b-f) denoised image using NLSPCA, NLPCA, Lee filter, Weiner filter, and WFT, respectively.

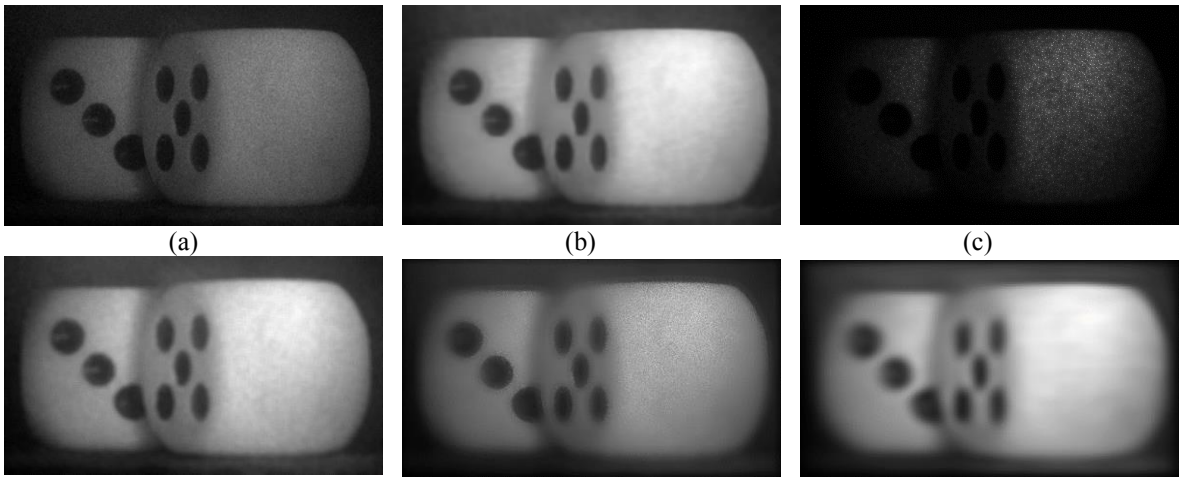

(a) (b) (c)

(d) (e) (f)

Fig. 11. Results of filtering for two-dice image reconstructed from the experimentally recorded digital hologram. (a) Original image, (b-f) denoised image using NLSPCA, NLPCA, Lee filter, Weiner filter, and WFT, respectively.

Fig. 12 shows a plot of the computed ENL values for the different filtering methods implemented for the two experimental data. The computed ENL values demonstrate the filtering capability of the NLS-PCA method. According to the histogram shown in Fig. 12, the superiority of the NLSPCA method is confirmed in comparison to other filtering techniques on the experimental data.

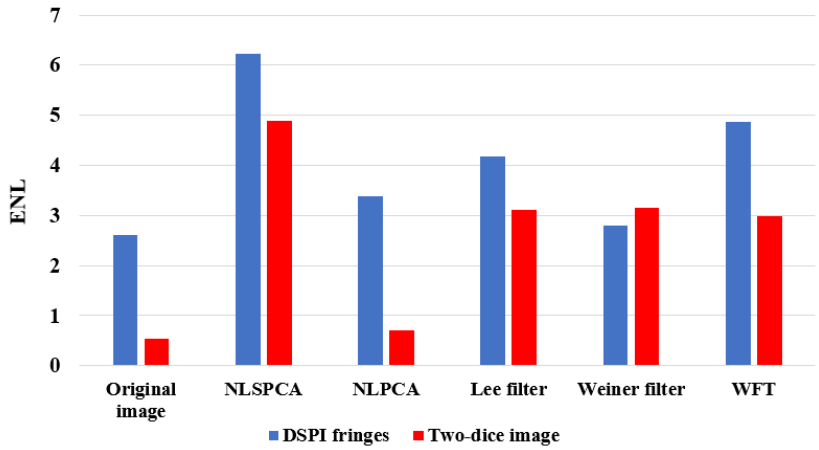

Fig. 10. ENL values plots for different filtering methods

5. Conclusion

The present research aims to examine the performance of the nonlocal sparse principal component analysis (NLS-PCA) for speckle noise reduction as applied to optical interferometric techniques. The study has shown that NLS-PCA performs very well and is able to obtain excellent speckle noise removal and edge preservation at low computational complexity when compared with the NL-PCA approach and some state-of-the-art methods from speckle fringe patterns and holographic images. The numerical simulation shows that a patch size of 5 and cluster numbers of 70 are the two principal parameters that significantly remove the speckle noise from the fringe patterns. The NLS-PCA method performs very well and preserves the fine details in all images including the closed fringes and at all levels of noise. Overall, based on the obtained results, it can be concluded that NLS-PCA method for speckle noise filtering is effective and could be established as a powerful speckle-noise filtering tool for optical imaging techniques.

Funding

Osamu Matoba acknowledges the support of a Grant-in-Aid for Scientific Research from the Japan Society for the Promotion of Science (20H05886).

References

1. Kim, Myung K. "Principles and techniques of digital holographic microscopy." SPIE reviews 1.1 (2010): 018005.
2. Kumar, Manoj, et al. "Common-path multimodal three-dimensional fluorescence and phase imaging system." Journal of biomedical optics 25.3 (2020): 032010.
3. Kemper, Björn, et al. "Investigation of living pancreas tumor cells by digital holographic microscopy." Journal of biomedical optics 11.3 (2006): 034005.
4. Quan, Xiangyu, et al. "Three-dimensional stimulation and imaging-based functional optical microscopy of biological cells." Optics letters 43.21 (2018): 5447-5450.
5. Park, YongKeun, et al. "Spectroscopic phase microscopy for quantifying hemoglobin concentrations in intact red blood cells." Optics letters 34.23 (2009): 3668-3670.
6. Kumar, Manoj, et al. "Digital holographic multimodal cross-sectional fluorescence and quantitative phase imaging system." Scientific Reports 10.1 (2020): 1-13.
7. Park, YongKeun, Christian Depeursinge, and Gabriel Popescu. "Quantitative phase imaging in biomedicine." Nature photonics 12.10 (2018): 578-589.
8. Kumar, Manoj, et al. "Single-shot common-path off-axis digital holography: applications in bioimaging and optical metrology." Applied Optics 60.4 (2021): A195-A204.
9. Nehmetallah, Georges, and Partha P. Banerjee. "Applications of digital and analog holography in three-dimensional imaging." Advances in Optics and Photonics 4.4 (2012): 472-553.
10. Kumar, Manoj, et al. "Single-shot common-path off-axis dual-wavelength digital holographic microscopy." Applied Optics 59.24 (2020): 7144-7152.
11. Quan, Xiangyu, et al. "Multimodal microscopy: fast acquisition of quantitative phase and fluorescence imaging in 3D space." IEEE Journal of Selected Topics in Quantum Electronics 27.4 (2020): 1-11.
12. Kumar, Manoj, et al. "Measurement of initial displacement of canine and molar in human maxilla under different canine retraction methods using digital holographic interferometry." Optical Engineering 57.9 (2018): 094106.
13. Kumar, Manoj, Gufran Sayeed Khan, and Chandra Shakher. "Measurement of elastic and thermal properties of composite materials using digital speckle pattern interferometry." SPECKLE 2015: VI International Conference on Speckle Metrology. Vol. 9660. SPIE, 2015.
14. Osten, Wolfgang, Torsten Baumbach, and Werner Jüptner. "Comparative digital holography." Optics letters 27.20 (2002): 1764-1766.
15. Sheridan, John T., et al. "Roadmap on holography." Journal of Optics 22.12 (2020): 123002.
16. Kumar, Manoj, et al. "Measurement of strain distribution in cortical bone around miniscrew implants used for orthodontic anchorage using digital speckle pattern interferometry." Optical Engineering 55.5 (2016): 054101.
17. Kumar, Manoj, Varun Kumar, and Chandra Shakher. "Measurement of temperature and temperature distribution in diffusion flames using digital speckle pattern interferometry." Eleventh International Conference on Correlation Optics. Vol. 9066. SPIE, 2013.
18. Kumar, Manoj, and Chandra Shakher. "Measurement of hygroscopic strain in deodar wood during convective drying using lensless Fourier transform digial holography." Optical Micro-and Nanometrology VI. Vol. 9890. SPIE, 2016.
19. Kumar, Manoj, and Chandra Shakher. "Experimental characterization of the hygroscopic properties of wood during convective drying using digital holographic interferometry." Applied optics 55.5 (2016): 960-968.
20. Kumar, Manoj, Kumresh Kumar Gaur, and Chandra Shakher. "Measurement of material constants (Young's modulus and Poisson's ratio) of polypropylene using digital speckle pattern interferometry (DSPI)." Journal of the Japanese Society for Experimental Mechanics 15.Special_Issue (2015): s87-s91.
21. Kumar, Manoj, and Osamu Matoba. "2D full-field displacement and vibration measurements of specularly reflecting surfaces by two-beam common-path digital holography." Optics Letters 46.23 (2021): 5966-5969.
22. Picart, Pascal, et al. "2D full field vibration analysis with multiplexed digital holograms." Optics express 13.22 (2005): 8882-8892.
23. Schnars, Ulf, and Werner Jüptner. "Direct recording of holograms by a CCD target and numerical reconstruction." Applied optics 33.2 (1994): 179-181.
24. Kumar M. Some novel applications of digital speckle pattern interferometry and digital holographic interferometry. Diss. 2016.
25. Kumar, Manoj, and Chandra Shakher. "Measurement of temperature and temperature distribution in gaseous flames by digital speckle pattern shearing interferometry using holographic optical element." Optics and Lasers in Engineering 73 (2015): 33-39.

26. Kumar, Manoj, et al. "Speckle denoising techniques in imaging systems." Journal of Optics 22.6 (2020): 063001.
27. Sagheer, Sameera V. Mohd, and Sudhish N. George. "A review on medical image denoising algorithms." Biomedical signal processing and control 61 (2020): 102036.
28. Singh, Prabhishek, et al. "A Review on SAR Image and its Despeckling." Archives of Computational Methods in Engineering 28.7 (2021): 4633-4653.
29. Baumbach, Torsten, et al. "Improvement of accuracy in digital holography by use of multiple holograms." Applied Optics 45.24 (2006): 6077-6085.
30. Rong, Lu, et al. "Speckle noise reduction in digital holography by use of multiple polarization holograms." Chinese Optics Letters 8.7 (2010): 653-655.
31. Zhou, Yi, and Hongguang Li. "Adaptive noise reduction method for DSPI fringes based on bi-dimensional ensemble empirical mode decomposition." Optics express 19.19 (2011): 18207-18215.
32. Xiao, Qiyang, Jian Li, and Zhoumo Zeng. "A denoising scheme for DSPI phase based on improved variational mode decomposition." Mechanical Systems and Signal Processing 110 (2018): 28-41.
33. Kemao, Qian. "Two-dimensional windowed Fourier transform for fringe pattern analysis: principles, applications and implementations." Optics and Lasers in Engineering 45.2 (2007): 304-317.
34. Yassine, Tounsi, Siari Ahmed, and Nassim Abdelkrim. "Speckle noise reduction in digital speckle pattern interferometry using Riesz wavelets transform." 2017 International Conference on Advanced Technologies for Signal and Image Processing (ATSIP). IEEE, 2017.
35. Ning, Xueling, et al. "Fast phase denoising using stationary wavelet transform in speckle pattern interferometry." Measurement Science and Technology 31.2 (2019): 025205.
36. Zada, Sara, et al. "Contribution study of monogenic wavelets transform to reduce speckle noise in digital speckle pattern interferometry." Optical Engineering 58.3 (2019): 034109.
37. Dabov, Kostadin, et al. "Image denoising with block-matching and 3D filtering." Image processing: algorithms and systems, neural networks, and machine learning. Vol. 6064. SPIE, 2006.
38. Tounsi, Yassine, et al. "Speckle noise reduction in digital speckle pattern interferometric fringes by nonlocal means and its related adaptive kernel-based methods." Applied Optics 57.27 (2018): 7681-7690.
39. Tounsi, Yassine, et al. "Speckle denoising by variant nonlocal means methods." Applied optics 58.26 (2019): 7110-7120.
40. Salmon, Joseph, et al. "Poisson noise reduction with non-local PCA." Journal of mathematical imaging and vision 48.2 (2014): 279-294.
41. Muresan, D. Darian, and Thomas W. Parks. "Adaptive principal components and image denoising." Proceedings 2003 International Conference on Image Processing (Cat. No. 03CH37429). Vol. 1. IEEE, 2003.
42. Lv, Hongli, et al. "Speckle noise reduction of multi-frame optical coherence tomography data using multi-linear principal component analysis." Optics Express 26.9 (2018): 11804-11818.
43. Farhadiani, Ramin, Saeid Homayouni, and Abdolreza Safari. "Hybrid SAR speckle reduction using complex wavelet shrinkage and non-local PCA-based filtering." IEEE Journal of Selected Topics in Applied Earth Observations and Remote Sensing 12.5 (2019): 1489-1496.
44. Alkinani, Monagi H., and Mahmoud R. El-Sakka. "Patch-based models and algorithms for image denoising: a comparative review between patch-based images denoising methods for additive noise reduction." EURASIP Journal on Image and Video Processing 2017.1 (2017): 1-27.
45. Zhang, Lei, et al. "Two-stage image denoising by principal component analysis with local pixel grouping." Pattern recognition 43.4 (2010): 1531-1549.
46. Deledalle, Charles-Alban, Joseph Salmon, and Arnak S. Dalalyan. "Image denoising with patch based PCA: local versus global." BMVC. Vol. 81. 2011.
47. Buades, Antoni, Bartomeu Coll, and Jean-Michel Morel. "Non-local means denoising." Image Processing On Line 1 (2011): 208-212.
48. Barj, E. M., et al. "Speckle correlation fringes denoising using stationary wavelet transform. Application in the wavelet phase evaluation technique." Optics & Laser Technology 38.7 (2006): 506-511.
49. Brunet, Dominique, Edward R. Vrscay, and Zhou Wang. "On the mathematical properties of the structural similarity index." IEEE Transactions on Image Processing 21.4 (2011): 1488-1499.
50. Johnstone, Iain M., and Arthur Yu Lu. "On consistency and sparsity for principal components analysis in high dimensions." Journal of the American Statistical Association 104.486 (2009): 682-693.
51. Qi, Xin, Ruiyan Luo, and Hongyu Zhao. "Sparse principal component analysis by choice of norm." Journal of multivariate analysis 114 (2013): 127-160.
52. Bernardo, Marco V., et al. "Holographic representation: Hologram plane vs. object plane." Signal Processing: Image Communication 68 (2018): 193-206.

Declaration of interests

☒The authors declare that they have no known competing financial interests or personal relationships that could have appeared to influence the work reported in this paper.

☐The authors declare the following financial interests/personal relationships which may be considered as potential competing interests: